

Weighing the Axion with Muon Haloscopy

N. Bray-Ali*
Science Synergy
 Los Angeles, CA 90045
 (Dated: November 2, 2023)

Recent measurements of muon spin precession confirm a long-standing tension with the Standard Model of particle physics. We argue that axions from the local dark matter halo of the galaxy are responsible for the tension. The argument yields a percent level prediction for the mass of the axion provided that dark matter is made of axions. An analysis of charge asymmetry in kaon decays suggests that at least in the local halo dark matter is made of axions and that axions from the local halo are responsible for the observed violation by these reactions of the combined charge conjugation and spatial inversion symmetry operation. Tabletop experiments to directly detect dark matter in the form of axions with the predicted mass are proposed.

Introduction—The spin of the muon precesses in a magnetic field B at frequency $\omega_a = a_\mu(e/m_\mu)B$, where, $a_\mu \approx \alpha/(2\pi) \approx 1.16 \times 10^{-3}$ is the electromagnetic leading order contribution to spin precession, and $e/m_\mu = 2\pi \times 135$ MHz/T is the charge to mass ratio of the muon [1–5]. Compared with the electron, the muon is $(m_\mu/m_e)^2 \approx 43,000$ times more sensitive to the hadronic leading order contribution $a_\mu^{\text{HLO}} \approx 700 \times 10^{-10}$ to spin precession [5, 6]. In this Article, we show that axions in the local dark matter halo of the galaxy shift a_μ and a_μ^{HLO} from their standard model values. Further, we argue that these axion-induced shifts resolve the tension between measurements of the muon spin precession frequency [2–4] and calculations of the frequency within the Standard Model [6–11] provided that dark matter in the local halo is made of axions as suggested by analysis of charge asymmetry between the kaon decay $K_L^0 \rightarrow \pi^+ e^- \bar{\nu}_e$ and its charge-parity conjugate $K_L^0 \rightarrow \pi^- e^+ \nu_e$ [12–16]. Finally, we give a physical picture for the nature of dark matter that leads to a prediction for the mass of the axion with percent level precision and we sketch table-top experiments for testing this prediction.

Nature of Dark Matter—We start by expressing the axion A_M in terms of quarks and leptons M_H^P with helicity $H = L, R$ and charge-parity check $P = +, -$ [18]:

$$A_M = M_L^- \bar{M}_R^- - M_R^- \bar{M}_L^- - M_L^+ \bar{M}_R^+ + M_R^+ \bar{M}_L^+ \quad (1)$$

Here, M runs over the twelve known “flavors” of quarks and leptons while the charge-parity check P is $+$ for quarks and leptons that do not feel the weak nuclear force and $-$ for those that do. In the standard model, we find M_L^- and M_R^+ , but neither M_L^+ nor M_R^- , where, L is for left-handed and R is for right-handed helicity [19].

Next, we suppose that axions A_M of each kind and photons γ_H of each helicity formed in equal numbers in the early universe prior to baryogenesis. This fixes the ratio $n_A/n_\gamma = |M|/|H| = 6$ of axions to photons and

gives the axion mass m_A ($\hbar = c = 1$) [20]:

$$m_A = 2.70 kT_\gamma \left(\frac{n_A}{n_\gamma} \right)^{-1} \frac{\Omega_A h^2}{\Omega_\gamma h^2} = (0.508 \pm 0.004) \text{ eV}, \quad (2)$$

where, $T_\gamma = (2.7255 \pm 0.0006)$ K is the present photon temperature [21], $\Omega_\gamma h^2 = 2.473 \times 10^{-5}$ is the photon energy density parameter and $\Omega_A h^2 = 0.11882 \pm 0.00086$ is that of dark matter [22].

Local Dark Matter Halo—The energy density of axions in the local dark matter halo of the galaxy ρ_A can be estimated using charge asymmetry of kaon decays [23]:

$$\begin{aligned} A_L(e) &= -2\sqrt{2}\xi_{A\pi} p_K \tilde{\phi}_A(q_A) \\ &= 4\pi C_{A\pi} \frac{f_\pi \sqrt{\rho_A \hbar c}}{m_A f_A} L_K, \end{aligned} \quad (3)$$

where, the axion amplitude $\tilde{\phi}_A(q_A)$ at momentum q_A changes sign under the combination of charge conjugation and space inversion probed by $A_L(e)$ to create the observed charge asymmetry [18]. The mixing angle $\xi_{A\pi} = -C_{A\pi} f_\pi / f_A$ between the axion A and the neutral pion π^0 can be expressed in terms of the pion decay constant $f_\pi = (92.32 \pm 0.09)$ MeV [24], the axion decay constant f_A [25], and the light quark masses using $C_{A\pi} = (m_d - m_u)/(2m_u + 2m_d) = (0.173 \pm 0.008)$ [26]. Here, the kaon beam has momentum p_K and decays in-flight within a detector of length L_K .

In contrast to the local axion energy density, the axion mass m_A and decay constant f_A only enter the kaon charge asymmetry through the product $m_A f_A = \sqrt{\chi_{\text{QCD}}} = (5.69 \pm 0.05) \times 10^{-3}$ GeV² which is fixed by the topological susceptibility χ_{QCD} of the quantum chromodynamic vacuum [27]. Using the kaon parameters $L_K = 500$ cm and $A_L(e) = (3.32 \pm 0.08) \times 10^{-3}$ from the current best charge asymmetry measurement [17], the local axion energy density $\rho_A = (0.28 \pm 0.03)$ GeV/cm³ that we find from Eq. (3) agrees with the best available estimate $\rho_{\text{DM}} = (0.30 \pm 0.03)$ GeV/cm³ of the energy density of the local dark matter halo [28]. This agreement suggests that axions saturate the local dark matter halo

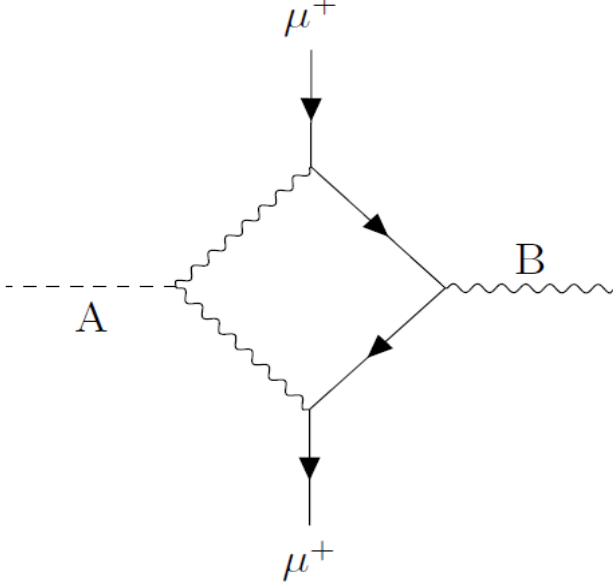


FIG. 1. Halo axion A collides with virtual photon or vector meson dressing vertex of positive muon μ^+ and magnetic field B .

and that dark matter from the local halo is the source of the charge asymmetry observed in kaon decays [29].

Muon Haloscopy—Figure 1 shows how axions in the local dark matter halo shift muon spin precession [3–5]. Acting as a background field $\tilde{\phi}_A(q_A)$ with on-shell four-momentum $q_A^2 = m_A^2 \ll m_\mu^2$, the axion A couples to the virtual photon dressing the vertex of the positive muon μ^+ and the magnetic field B . The axion-photon coupling of strength $g_{A\gamma\gamma} = (0.68 \pm 0.02) \times 10^{-10} \text{ GeV}^{-1}$ [30] changes the photon's Green's function [31, 32]

$$\Delta D_+(x, x') = m_A^2 g_{A\gamma\gamma} \tilde{\phi}_A(q_A) D_+(x, x'), \quad (4)$$

and this change in the photon propagator produces the shift of the spin precession frequency [33]:

$$\begin{aligned} \frac{\Delta a_\mu}{a_\mu} &= m_A^2 g_{A\gamma\gamma} \tilde{\phi}_A(q_A) \\ &= \pm m_A g_{A\gamma\gamma} \sqrt{\rho_A N_\mu V_\mu T_\mu} \end{aligned} \quad (5)$$

where, the axion field strength $|\tilde{\phi}_A(q_A)|^2 \approx \phi_A^2 N_\mu V_\mu T_\mu$ is fixed by the axion energy density $\rho_A = \phi_A^2 m_A^2$, the volume V_μ of the muon beam, the lifetime T_μ of the muon in the axion rest-frame, and the average number of muons N_μ during spin precession.

The sign of the axion-driven shift Δa_μ of the muon spin precession frequency switches along with the axion field $\tilde{\phi}_A(q_A)$ under spatial inversion P , under time-reversal T , and under the combinations CP and CT with charge conjugation C [34]. The size of the shift scales with muon

beam parameters [37]

$$\begin{aligned} \frac{\Delta a_\mu}{a_\mu} &= (165 \pm 10) \times 10^{-11} \left(\frac{N_\mu}{1930} \right)^{1/2} \left(\frac{\sigma_x}{1.78 \text{ cm}} \right)^{1/2} \\ &\times \left(\frac{\sigma_y}{1.25 \text{ cm}} \right)^{1/2} \left(\frac{R}{711 \text{ cm}} \right)^{1/2} \left(\frac{T_\mu}{64.4 \text{ } \mu\text{sec}} \right)^{1/2} \end{aligned} \quad (6)$$

where, σ_x is the width of the muon beam, σ_y is its height, and R is the radius of the storage ring. This has roughly the right size to resolve the 3.4σ tension between the spin precession experiments (Exp) [2–4] and standard model calculations (SM) [6–11]

$$a_\mu(\text{Exp}) - a_\mu(\text{SM}) = (140 \pm 41) \times 10^{-11}, \quad (7)$$

where, we have used the recently emerged consensus value $a_\mu^{\text{HLO}}(\text{SM}) = (704.1 \pm 3.0) \times 10^{-10}$ [35] for the leading order hadronic contribution to the muon spin precession frequency within the Standard Model [36]. Using the muon parameters, we estimate the axion shift [37]

$$\Delta a_\mu = (165 \pm 10) \times 10^{-11}. \quad (8)$$

The pleasing agreement of the axion shift Δa_μ and the observed gap $a_\mu(\text{Exp}) - a_\mu(\text{SM})$ resolves the 3.4σ tension between the Standard Model and the muon spin precession measurements.

Hadronic Haloscopy—Figure 1 also shows how axions from the local dark matter halo of the galaxy shift measurements of the leading order hadronic contribution a_μ^{HLO} to muon spin precession [5, 6]. Acting as a background field, the axions couple to the ρ^0 vector meson that dominates the hadronic production from electron-positron annihilation whose cross-section enters the standard model calculation of a_μ^{HLO} [38]. The axion coupling converts the short-lived ρ^0 meson, which produces mainly charged pion $\pi^+ \pi^-$ pairs, into the longer lived and slightly heavier ω meson which prefers to produce a neutral pion π^0 in addition to the charged pion pair [39].

Dark matter-driven conversions of the neutral ρ^0 vector meson into the isoscalar ω vector meson reduce the resonant charged pion pair production cross-section that enters the resonant part $a_\mu^{\pi\pi} \approx 380 \times 10^{-10}$ [8] of the hadronic leading order contribution a_μ^{HLO} [40]. The axion-meson coupling $g_{A\rho\omega} = 898 g_{A\gamma\gamma} = (6.11 \pm 0.18) \times 10^{-8} \text{ GeV}^{-1}$ [41] then leads to the shift [42]:

$$\begin{aligned} \frac{\Delta a_\mu^{\pi\pi}}{a_\mu^{\pi\pi}} &= m_A E_\rho g_{A\rho\omega} \tilde{\phi}_A(q_A) \\ &= \frac{g_{A\rho\omega}}{g_{A\gamma\gamma}} \frac{\Delta a_\mu}{a_\mu} \frac{E_\rho}{m_A} \sqrt{\frac{1}{N_\mu} \frac{V_\rho T_\rho}{V_\mu T_\mu}}, \end{aligned} \quad (9)$$

where, E_ρ is the vector meson energy in the axion rest frame, V_ρ is the luminous volume created by the colliding electron and positron bunches, and T_ρ is the time it

takes the bunches to cross during the collision. The beam parameters give the axion shift [41, 43]

$$\Delta a_{\mu}^{\pi\pi} = (19.6 \pm 1.2) \times 10^{-11} \left(\frac{E_{\rho}}{1000 \text{ MeV}} \right) \left(\frac{\sigma_x}{100 \text{ } \mu\text{m}} \right)^{1/2} \times \left(\frac{\sigma_y}{10 \text{ } \mu\text{m}} \right)^{1/2} \left(\frac{\sigma_z}{1 \text{ cm}} \right), \quad (10)$$

where, σ_x is the width of the electron and positron bunches, σ_y is their height, and σ_z their length.

The emerging consensus for the Standard Model value of the muon spin precession frequency includes the determination of the resonant part of the hadronic contribution $a_{\mu}^{\pi\pi}$ (CMD3) by the CMD-3 collaboration [8]. The previous consensus was dominated by the KLOE collaboration result $a_{\mu}^{\pi\pi}$ (KLOE) [44–47]. The two values disagree by 5.1 standard deviations [48]

$$a_{\mu}^{\pi\pi}(\text{CMD3}) - a_{\mu}^{\text{HLO}}(\text{KLOE}) = (188 \pm 37) \times 10^{-11}. \quad (11)$$

Using Eq. (10) with the KLOE and CMD beam parameters gives a relative axion shift of roughly the right size to resolve the discrepancy [49]

$$\Delta a_{\mu}^{\pi\pi}(\text{KLOE}) - \Delta a_{\mu}^{\pi\pi}(\text{CMD3}) = (167 \pm 10) \times 10^{-11}. \quad (12)$$

The pleasing agreement between the relative axion shift $\Delta a_{\mu}^{\pi\pi}(\text{KLOE}) - \Delta a_{\mu}^{\pi\pi}(\text{CMD3})$ and the observed gap $a_{\mu}^{\pi\pi}(\text{CMD3}) - a_{\mu}^{\text{HLO}}(\text{KLOE})$ resolves the 5.1 σ discrepancy between the two best determinations of the dominant part $a_{\mu}^{\pi\pi}$ of the hadronic leading order contribution to the muon spin precession frequency within the Standard Model.

Proton Haloscopy—Inverting the process shown in Figure 1 about a horizontal axis and replacing the muon with a proton, we find the way that axions from the local dark matter halo of the galaxy shift the spin precession of protons in the molecules of a liquid during nuclear magnetic resonance [50]:

$$\Delta g'_p = \frac{\alpha}{\pi\epsilon} m_A^2 g_{A\gamma\gamma} \tilde{\phi}_A(q_A) = 2 \frac{\Delta a_{\mu}}{\epsilon} \sqrt{\frac{N_p V_p T_p}{N_{\mu} V_{\mu} T_{\mu}}}, \quad (13)$$

where, ϵ is the static dielectric constant of the liquid and $g'_p \approx 5.58$ gives the proton spin precession frequency $\omega'_p = (g'_p/2)(e/m_p)B \approx 2\pi \times 42.8 \text{ MHz/T} \times B$ for magnetic field B [51]. Here, N_p is the effective number of protons, V_p is the volume containing the protons, and $T_p = 1/\Delta\omega'_p$ is the effective coherence time of the proton spin precession due to the broadening $\Delta\omega'_p$ of the resonance by variations in the field strength over the sample volume. Straightforward estimates of the proton parameters give the slope of the axion shift of the proton spin

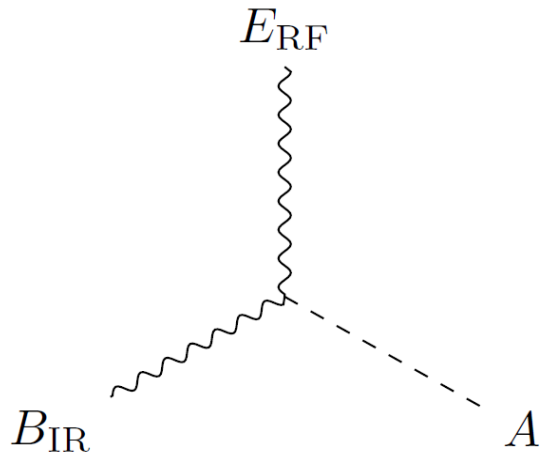


FIG. 2. Dark matter A from the local halo of the galaxy converts infrared magnetic field B_{IR} into radio-frequency electric field E_{RF} that drives electron cyclotron motion and microwave cavity resonance.

precession frequency [52]

$$\frac{1}{g'_p} \frac{dg'_p}{dT} = -(10.0 \pm 0.6) \frac{\text{ppb}}{\text{K}} \left(\frac{\epsilon}{78.4} \right)^{-1} \left(\frac{\rho}{1 \text{ g/cm}^3} \right)^{1/2} \times \left(\frac{\mu}{9 \text{ g/mol H}} \right)^{-1/2} \left(\frac{T}{300 \text{ K}} \right)^{-3/2} \left(\frac{V_p}{0.62 \text{ cm}^3} \right) \times \left(\frac{\Delta\omega'_p}{2.6 \times 10^{-7} \omega'_p} \right)^{-1/2}, \quad (14)$$

where, T is the temperature, ρ is the density, and μ is the mass of the liquid containing a mole of protons. Measurements of proton spin precession in liquids with the necessary precision to see the dark matter shift were achieved half a century ago [51]. Verifying the proton parameter dependence shown in Eq. (14) of the slope dg'_p/dT would directly confirm in a tabletop experiment the proposed mechanism for the shift of spin precession by axions from the local dark matter halo with the predicted mass.

Atomic Haloscopy—Replacing the positive muon in Figure 1 with the valence electron of an atom with large atomic number trapped in an optical lattice and replacing the external magnetic field with the internal magnetic field within the atom [53], we find the process that shifts the electromagnetic fine-structure coupling constant α felt by the electron during transitions among valence states:

$$\frac{\Delta\alpha}{\alpha} = m_A^2 g_{A\gamma\gamma} \tilde{\phi}_A(q_A) = \frac{\Delta a_{\mu}}{a_{\mu}} \sqrt{\frac{N_a V_a T_a}{N_{\mu} V_{\mu} T_{\mu}}}, \quad (15)$$

where, N_a is the number of atoms trapped in the optical lattice, V_a is the trap volume, and T_a is the coherence time for the motion of the ultracold atoms. The shift in α leads to a density-shift of the optical lattice clock

frequency [54]:

$$\begin{aligned} \frac{\Delta\nu}{\nu} &= k_\alpha \frac{\Delta\alpha}{\alpha} = (11.8 \pm 0.7) \times 10^{-17} \left(\frac{N_a}{100} \right)^{1/2} \\ &\times \left(\frac{V_0}{200 E_R} \right)^{-3/4} \left(\frac{T}{9 \mu\text{K}} \right)^{1/4} \left(\frac{k_\alpha}{0.24} \right) \\ &\times \left(\frac{E_R}{\hbar \times 2.0 \text{ kHz}} \right)^{-3/2} \left(\frac{m}{171 m_p} \right)^{-3/4} \left(\frac{w}{26.4 \lambda_L} \right) \end{aligned} \quad (16)$$

where, k_α is the sensitivity of the transition frequency to shifts in the fine-structure constant, $E_R = \hbar^2/(2m\lambda_L^2)$ is the kinetic energy with which the atoms of mass m recoil when they spontaneously emit photons at the wavelength λ_L of the optical lattice, V_0 is the lattice depth, w is the lattice laser beam waist, and T is the temperature of the atoms in the trap. By modulating the number of atoms in the trap, a density shift of the optical lattice clock frequency of this size can be readily observed [55].

Cyclotron Haloscopy—Figure 2 shows how dark matter drives electron cyclotron motion by converting infrared laser photons near the Compton wavelength $\lambda_A = 2\pi/m_A = (2441 \pm 19)$ nm into radio-frequency electromagnetic waves within a magnetically confined plasma. When the beat note between the infrared light and the Compton wavelength of dark matter hits the electron cyclotron resonance frequency $\omega_c = (e/m_e)B = 2\pi \times 28$ GHz ($B/1$ T) for the magnetic field of strength B that confines the plasma, the radio-frequency electric field created by the interference heats the electrons at the rate [56]

$$\begin{aligned} P_{\text{RF}} &= \frac{P_{\text{IR}}}{2} m_A^4 g_{A\gamma\gamma}^2 |\tilde{\phi}_A(q_A)|^2 \\ &= \frac{P_{\text{IR}}}{2} \left(\frac{\Delta a_\mu}{a_\mu} \right)^2 \frac{n_e V_e}{N_\mu} \frac{V_e T_e}{V_\mu T_\mu} \end{aligned} \quad (17)$$

where, P_{IR} is the infrared power sent into the plasma, n_e is the density of plasma electrons, V_e is the volume of the infrared beam within the plasma, and T_e is set by the coherence time of the infrared light. For typical laser [57] and plasma parameters [58], the resonant heating of the plasma leads to a drop in the transmitted infrared power that can be readily observed [59]

$$\begin{aligned} \frac{\Delta P_{\text{IR}}}{P_{\text{IR}}} &= (6.5 \pm 0.8)\% \left(\frac{\Delta\nu_{\text{IR}}}{1 \text{ MHz}} \right)^{-1} \left(\frac{\beta}{0.8} \right) \\ &\times \left(\frac{T}{12,000 \text{ K}} \right)^{-1} \left(\frac{L}{100 \text{ cm}} \right)^2 \left(\frac{B}{0.32 \text{ T}} \right)^{-2}, \end{aligned} \quad (18)$$

where, $\Delta\nu_{\text{IR}}$ is the coherent line-width of the infrared laser, β is the ratio of the electron pressure to the magnetic energy density in the plasma, T is the temperature of the plasma, and L is the laser path length through the plasma.

Microwave Haloscopy—Figure 2 also shows how the infrared magnetic field B_{IR} of laser photons passing

through a microwave cavity converts under the influence of axions from the local dark matter halo of the galaxy into the radio-frequency electric field E_{RF} that excites the cavity to resonate with power [56]

$$P_{\text{RF}} = \frac{1}{2} P_{\text{IR}} \left(\frac{\Delta a_\mu}{a_\mu} \right)^2 \frac{1}{N_\mu} \frac{V_{\text{IR}} T_{\text{IR}}}{V_\mu T_\mu}, \quad (19)$$

where, P_{IR} is the infrared laser power, V_{IR} is the volume of the infrared laser beam within the microwave cavity, and T_{IR} is the coherence time of the infrared laser. For a receiver at noise temperature T_S and a search that takes total time T_A , the radio-frequency power gives resonant signal-to-noise ratio [60]

$$\begin{aligned} \text{SNR} &= (10.0 \pm 1.2) \left(\frac{P_{\text{IR}}}{3 \text{ mW}} \right) \left(\frac{\Delta\nu_{\text{IR}}}{1 \text{ MHz}} \right)^{-1} \left(\frac{D}{1 \text{ cm}} \right)^2 \\ &\times \left(\frac{T_A}{10^6 \text{ sec}} \right)^{1/2} \left(\frac{L}{112 \text{ cm}} \right) \left(\frac{T_S}{77 \text{ K}} \right)^{-1}, \end{aligned} \quad (20)$$

where, $\Delta\nu_{\text{IR}} = 1/(2\pi T_{\text{IR}})$ is the infrared laser line-width, D is the beam diameter, and L is the length of the cavity. For typical laser [57] and cavity [61] parameters, the mass of the axion can be determined with precision $\hbar\Delta\nu_{\text{IR}}/(m_A c^2) = 8.2$ ppb that is more than double that of the mass of the muon $\Delta m_\mu/m_\mu = 22$ ppb [12] in a search time $T_A = 10^6$ sec ≈ 12 days that takes less than a month.

Bend Magnet Haloscopy—Replacing the infrared magnetic field in Figure 2 with the static magnetic field B_{DC} of a dipole bend magnet and swapping the radio-frequency electric field for an infrared electric field E_{IR} , we find the process for converting axions from the local dark matter halo of the galaxy into photons with infrared power [62]

$$P_{\text{IR}} = S_{\text{IR}} \left(\frac{B_{\text{DC}}^2 c^2}{2Z_0} \right) \left(\frac{\Delta a_\mu}{a_\mu} \right)^2 \frac{1}{N_\mu} \frac{V_{\text{IR}} T_{\text{IR}}}{V_\mu T_\mu}, \quad (21)$$

where, S_{IR} is the photosensitive area of the infrared detector, V_{IR} is the volume of the resonant cavity formed by placing infrared mirrors at the entrance and exit of the bend magnet, and $T_{\text{IR}} = 1/(2\pi\Delta\nu_{\text{IR}})$ is the coherence time of the infrared laser with line-width $\Delta\nu_{\text{IR}}$ that is used to tune the cavity to the resonance frequency $\omega_A = m_A c^2/\hbar = 2\pi \times (122.7 \pm 1.0)$ THz set by the rest-mass of dark matter. Scanning the infrared frequency through this window of width $\Delta\omega_A = 2\pi \times 1.0$ THz allows the resonance to be found in a search time T_A with signal-to-noise ratio [63]

$$\begin{aligned} \text{SNR} &= (10.2 \pm 1.2) \\ &\times \left(\frac{S_{\text{IR}}}{2.83 \times 10^{-5} \text{ m}^2} \right) \left(\frac{B_{\text{DC}}}{1 \text{ T}} \right)^2 \left(\frac{D}{1 \text{ cm}} \right)^2 \\ &\times \left(\frac{L}{100 \text{ cm}} \right) \left(\frac{\Delta\nu_{\text{IR}}}{1 \text{ MHz}} \right)^{-1/2} \left(\frac{T_A}{17.4 \text{ hr}} \right)^{1/2} \end{aligned} \quad (22)$$

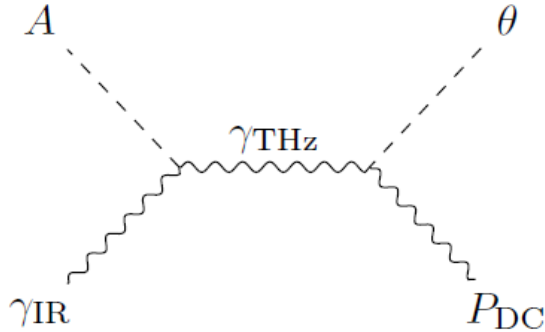


FIG. 3. Halo axion A converts infrared photon γ_{IR} into terahertz photon γ_{THz} resonant with electromagnon θ in ferroelectric antiferromagnet with polarization P_{DC} .

$$\times \left(\frac{\text{NEP}_A}{5.3 \times 10^{-13} \text{ W/Hz}^{1/2}} \right)^{-1},$$

where, D is the laser beam diameter used to tune the cavity, L is the length of the bend magnet, and NEP_A is the noise equivalent power of the infrared detector at the Compton wavelength of dark matter $\lambda_A = (2.44 \pm 0.02) \mu\text{m}$. For typical detector [64] and magnet [65] parameters, the signal-to-noise ratio suffices to directly detect the resonant conversion of dark matter to infrared photons and measure the mass of the axions with precision $2\pi\Delta\nu_{\text{IR}}/\omega_A = 8.2$ ppb using a typical line-width $\Delta\nu_{\text{IR}} = 1$ MHz [57] and a search time $T_A = 17.4$ hr taking less than a day.

Electromagnon Haloscopy— Figure 3 shows how the axion allows infrared light to excite electromagnons in ferroelectric antiferromagnets such as BiFeO_3 [66]. At room temperature the strongest electromagnon resonance in BiFeO_3 lies in the terahertz regime at frequency $\omega_\theta = 2\pi \times 0.54$ THz [67]. Looking in the infrared, we expect to see the electromagnon resonance as an absorption line in transmission through a sample provided the infrared light is detuned by ω_θ from the axion frequency $\omega_A = m_A = 2\pi \times (122.7 \pm 1.0)$ THz [68].

Measuring the infrared frequency $\omega_{A\theta} = \omega_A - \omega_\theta$ that resonantly excites the electromagnon provides a table-top determination of the mass of the axion. For a thin sample, the dip in infrared transmission on resonance at $\omega_{A\theta}$ is set by the infrared refractive index $n(\omega_{A\theta})$ and the infrared absorption coefficient [69]:

$$\begin{aligned} \frac{\alpha(\omega_{A\theta})}{\alpha(\omega_\theta)} &= (n(\omega_{A\theta}))^2 m_A^4 g_{A\gamma\gamma}^2 |\tilde{\phi}_A(q_A)|^2 \quad (23) \\ &= (n(\omega_{A\theta}))^2 \left(\frac{\Delta a_\mu}{a_\mu} \right)^2 \frac{n_\theta V_\theta}{N_\mu} \frac{V_\theta T_\theta}{V_\mu T_\mu}, \end{aligned}$$

where, n_θ is the density of electrons participating in the electromagnon mode, V_θ is the volume of the infrared beam within an optically thin sample, and $T_\theta = 1/\Delta\omega_\theta$

is the coherent life-time of the electromagnon with line-width $\Delta\omega_\theta$ and terahertz absorption coefficient $\alpha(\omega_\theta)$. Using typical electromagnon parameters, we find the infrared absorption coefficient of the resonance [70]

$$\begin{aligned} \alpha(\omega_{A\theta}) &= (12.4 \pm 1.5) \text{ cm}^{-1} \left(\frac{\alpha(\omega_\theta)}{10^7 \text{ cm}^{-1}} \right) \left(\frac{n(\omega_{A\theta})}{10} \right)^2 \\ &\times \left(\frac{n_\theta}{1.6 \times 10^{22} \text{ cm}^{-3}} \right) \left(\frac{V_\theta}{7.1 \times 10^{-3} \text{ cm}^3} \right)^2 \left(\frac{T_\theta}{30 \text{ ps}} \right) \end{aligned}$$

The resulting infrared absorption at the axion resonance in BiFeO_3 and related materials is large enough to be observable with readily available infrared spectrometers.

Conclusion— We conclude that the tensions between measurements of muon spin precession and standard model calculations are due to axions from the local dark matter halo of the galaxy. The resolution of the muon tension rests on a novel physical picture for the nature of dark matter. The picture leads to percent level predictions for the mass of the axion and for its coupling to electromagnetic fields.

Using kaon decays, we showed that dark matter in the local halo of the galaxy is made of axions. The observed charge asymmetry in kaon decays agrees with the asymmetry created by axions provided the axions have energy density that matches that of the local dark matter halo. The agreement suggests that the kaon decay asymmetry is due to axions in the local dark matter halo and that the local halo is made of axions.

The shift in the muon spin precession frequency due to axions from the local dark matter halo depends not just on the local axion energy density but also on the axion mass and electromagnetic coupling strength. For the mass of the axion predicted by our novel physical picture of the nature of dark matter, the predicted shift in the muon spin precession resolves the tension between precession measurements and Standard Model calculations. In addition, axions from the local dark matter halo convert the neutral vector meson that dominates photon-hadron interactions into its slightly heavier and less dominant isoscalar cousin. The resulting axion-driven shift of the measurements of the leading order hadronic contribution to muon spin precession resolves the 5.1σ discrepancy between the measurements that dominated the previous consensus [6, 44–47] and the more recent measurements that are part of the emerging consensus for the Standard Model value [8, 35].

We have proposed table-top experiments to confirm that dark matter is made of axions. We predict a temperature shift of the proton spin precession frequency in liquids and a density shift of the electron transition frequency in optical lattice clocks. The predicted size of both effects is large enough to be seen with presently available table-top experiments.

To directly measure the mass of the axion, we propose to beat dark matter from the local halo against in-

frared light at the predicted Compton wavelength. The interference creates electromagnetic waves that excite the electromagnon mode in materials such as the room-temperature multiferroic material BiFeO₃ and that drive electron cyclotron motion in a magnetically confined laboratory plasma. The predicted size of the resonant infrared electromagnon absorption coefficient and the predicted size of the electron cyclotron resonance heating in the plasma are both large enough to be seen in currently available table-top experiments.

Finally, we have proposed to use a bend magnet to create infrared photons and to use a microwave cavity to absorb such photons from axions in the local dark matter halo of the galaxy. Measuring the frequency of the infrared photons created by the magnet and absorbed by the cavity gives the mass of dark matter with more than twice the precision of the mass of the muon in searches that take less than a day with the magnet and less than a month with the cavity. These table-top experiments would confirm the proposed form of dark matter with the predicted mass.

Acknowledgements—This research was supported in part by the National Science Foundation under Grant No. NSF PHY-1748958, by the Department of Energy under grant No. DE-FG02-00ER41132, and by the Mainz Institute of Theoretical Physics within the Cluster of Excellence PRISMA+ (Project ID 39083149).

* nbrayali@gmail.com

- [1] J. Schwinger, Phys. Rev. **73**, 416 (1948).
- [2] D. P. Aguillard *et al.* (Muon $g - 2$ Collaboration), arXiv:2308.06230 [hep-ex] (2023).
- [3] B. Abi *et al.* (Muon $g - 2$ Collaboration), Phys. Rev. Lett. **126**, 141801 (2021).
- [4] G.W. Bennett *et al.* (Muon $g - 2$ Collaboration), Phys. Rev. D **73**, 072003 (2006).
- [5] F. Jegerlehner, *The Anomalous Magnetic Moment of the Muon*, 2nd ed., Springer-Verlag, Berlin (2017).
- [6] T. Aoyama *et al.* (Muon $g - 2$ Theory Initiative), Phys. Rep. **887**, 1 (2020).
- [7] Sz. Borsanyi *et al.* (BMW Collaboration), Nature **593**, 51 (2021).
- [8] F. V. Ignatov *et al.* (CMD-3 Collaboration), arXiv.org: 2302.08834 [hep-ex].
- [9] M. Fujikawa *et al.* (BELLE Collaboration), Phys. Rev. D **78**, 072006 (2008), arXiv:0805.3773 [hep-ex].
- [10] S. Schael *et al.* (ALEPH Collaboration), Phys. Rept. **421**, 191 (2005), arXiv:hep-ex/0506072 [hep-ex].
- [11] M. Davier, A. Hoecker, B. Malaescu, C.-Z. Yuan, and Z. Zhang, Eur. Phys. J. C **74**, 2803 (2014). For the result $a_\mu^{\text{HLO}}(\rho^\pm) = (703.0 \pm 4.4) \times 10^{-10}$, see Ref. [6], pg. 32 below Eq. (2.13).
- [12] P. A. Zyla *et al.* (Particle Data Group), Review of Particle Physics, Prog. Theor. Exp. Phys., **2020** 083C01 (2020).
- [13] S. Bennett *et al.*, Phys. Rev. Lett. **19**, 993 (1967).
- [14] J. Marx *et al.*, Phys. Lett. B **32**, 219 (1970).
- [15] V. L. Fitch *et al.* Phys. Rev. Lett. **31**, 1524 (1973).
- [16] C. Geweniger *et al.*, Phys. Lett. B **48**, 483 (1974).
- [17] A. Alavi-Harati *et al.* (FNAL KTeV Collab.), Phys. Rev. Lett. **88**, 181601 (2002).
- [18] The axions A_M are constructed to transform under C , P , and T as follows:
- $$CA_M = A_M, PA_M = -A_M, TA_M = -A_M. \quad (24)$$
- To check that they do so, recall that quarks and leptons M_H^P transforms as follows:
- $$CM_H^P = \overline{M}_H^{\overline{P}}, PM_H^P = M_H^{\overline{P}}, TM_H^P = \overline{M}_H^{\overline{P}}. \quad (25)$$
- [19] For anti-matter, the meaning of the parity check is reversed compared to matter: $P = +$ indicates anti-quarks and anti-leptons which *do* feel the weak force, while $P = -$ means the anti-matter *does not* feel it. Nevertheless, the standard model correlation between helicity $H = L, R$ and parity check $P = +, -$ applies in the same way to anti-matter as it does to matter: \overline{M}_L^- and \overline{M}_R^+ occur in the standard model while neither \overline{M}_L^+ nor \overline{M}_R^- do. See, for example, the discussion in Ref. [71] on pgs. 704–705.
- [20] There are $|M| = 12$ flavors of matter in the standard model of particle physics. They fall into three “generations” each containing a pair of quarks and a pair of leptons. See the discussion in Ref. [71] on pgs. 703–705, 707, and 721 for a detailed description of the matter content of the Standard Model in the language of quantum field theory. The ratio of the energy density parameters $\Omega_A h^2 / (\Omega_\gamma h^2) = u_A / u_\gamma$ gives the ratio of the energy per volume $u_A = m_A n_A$ stored in dark matter to the energy per volume $u_\gamma = 2.70 \times n_\gamma k T_\gamma$ stored in light energy. For a derivation, see P. J. E. Peebles, *Principles of Physical Cosmology*, Princeton University Press, Princeton, NJ (1993), pgs. 137–138, 158–160. The Boltzmann constant is [72]:
- $$\begin{aligned} k &= 1.380\,649 \times 10^{-23} \text{ J/K (exact)} \\ &= 0.861\,733 \times 10^{-4} \text{ eV/K.} \end{aligned}$$
- [21] D. J. Fixsen, Astrophys. J. **707**, 916 (2009).
- [22] N. Aghanim *et al.* (Planck Collaboration), A&A **641**, A6 (2018). We use parameters from the baseline model fit to the most complete combination of available data. The results are given in *Planck 2018 Results: Cosmological Parameter Tables*, pg. 49 (May 14, 2019).
- [23] The rate $\Gamma(\pi^- e^+ \nu_e)$ of the decay of the long-lived neutral kaon K_L^0 to a negative pion π^- , a positron e^+ , and an electron neutrino ν_e is larger than the rate $\Gamma(\pi^+ e^- \overline{\nu}_e)$ for the charge conjugate reaction due to the charge asymmetry [12]:
- $$\begin{aligned} A_L(e) &= \frac{\Gamma(\pi^- e^+ \nu_e) - \Gamma(\pi^+ e^- \overline{\nu}_e)}{\Gamma(\pi^- e^+ \nu_e) + \Gamma(\pi^+ e^- \overline{\nu}_e)} \\ &= (3.34 \pm 0.07) \times 10^{-3}. \end{aligned} \quad (26)$$
- The axion field strength $|\tilde{\phi}_A(q_A)|^2 \approx \phi_A^2 V_K T_K$ is fixed by the axion energy density $\rho_A = \phi_A^2 m_A^2$ where ϕ_A is the axion amplitude as a function of position [25]. The kaon volume $V_K = \pi L_K (h/p_K)^2$ and the kaon time $T_K = L_K/c$ give the size of the region of space-time within the decay volume where the axion and kaon interact coherently.

The following exact values for the defining constants of the international system (SI) appear in the expression for $A_L(e)$ and/or in its numerical evaluation [72]:

$$\begin{aligned} c &= 299\,792\,458 \text{ m/s,} \\ h &= \hbar \times 2\pi = 6.626\,070\,15 \times 10^{-34} \text{ J s,} \\ e &= 1.602\,176\,634 \times 10^{-19} \text{ C.} \end{aligned}$$

- [24] J. L. Rosner, S. L. Stone and R. Van de Water, 71. *Leptonic decays of charged pseudoscalar mesons*, pg. 803 in Ref. [12] gives the result $|V_{ud}|f_\pi \times \sqrt{2} = 127.13 \pm 0.13$ MeV where $|V_{ud}| = 0.973\,70 \pm 0.000\,14$ is the light quark mixing amplitude [73]. Combining we find $f_\pi = (92.32 \pm 0.09)$ MeV for the pion decay constant.
- [25] R. D. Peccei, in *CP Violation*, ed. C. Jarlskog, World Scientific, Singapore (1989), pgs. 525–532.
- [26] $C_{A\pi}$ follows from the way that the axial phase rotation symmetry of the axion $U_\theta^A A_M = A_M$ acts on the matter fields: $U_\theta^A M_H^P = e^{iP\theta} M_H^P$. See Ref. [25] for $C_{A\pi}$ in terms of the light quark mass ratio and the way that the axial phase rotation symmetry acts on the matter fields. See Ref. [74] for the light quark mass ratio $m_u/m_d = 0.485 \pm 0.019$.
- [27] M. Gorghetto and M. Villadoro, J. High Energ. Phys. **2019**, 33 (2019).
- [28] A.-C. Eilers, D. W. Hogg, H.-W. Rix, and M. K. Ness, *Astrophys. J.* **871**, 120 (2019).
- [29] Using the value for $\rho_A = (0.28 \pm 0.03)$ GeV/cm³ determined by the best available $A_L(e)$ measurement in Ref. [17], one can use Eq. (3) to predict the charge asymmetry observed in other experiments given the length L_K of their decay volume. For example, the first such measurement $A_L(e) = (2.24 \pm 0.36) \times 10^{-3}$ [13] had length $L_K = 375$ cm which yields $A_L(e) = (2.46 \pm 0.17) \times 10^{-3}$ using Eq. (3) in pleasing agreement with the observed charge asymmetry despite the well-known tension of this first measurement with the current world average. The difference in the length L_K resolves the tension. The rough similarity in the length $L_K \approx 500$ cm of the measurements that enter the current world average for which published scale drawings of the decay volume are available [14, 16, 17] explains the consistency of their results for $A_L(e)$ given the relation with L_K expressed in Eq. (3).
- [30] The axion-photon coupling is given by the following expression [25, 31]:

$$g_{A\gamma\gamma} = C_{A\gamma} \frac{\alpha}{2\pi} \frac{1}{f_A} = (0.68 \pm 0.02) \times 10^{-10} \text{ GeV}^{-1}. \quad (27)$$

Here, the fine-structure constant enters [72]:

$$\alpha = (7.297\,352\,5693 \pm 0.000\,000\,00011) \times 10^{-3}. \quad (28)$$

The mass of the axion m_A and the product $m_A f_A = \sqrt{\chi_{\text{QCD}}}$ which is fixed by the topological susceptibility χ_{QCD} of the quantum chromodynamic vacuum combine to give the axion decay constant [27]:

$$\begin{aligned} f_A = \frac{m_A f_A}{m_A} &= \frac{(5.69 \pm 0.05) \times 10^{-3} \text{ GeV}^2}{(0.508 \pm 0.004) \text{ eV}} \\ &= (1.120 \pm 0.010) \times 10^7 \text{ GeV.} \end{aligned} \quad (29)$$

Finally, the light quark mass ratio $m_u/m_d = 0.485 \pm 0.019$ [74] gives the dimensionless constant [25, 31]:

$$C_{A\gamma} = \frac{8}{3} - \frac{2}{3} \frac{4m_d + m_u}{m_d + m_u} = 0.653 \pm 0.017. \quad (30)$$

- [31] The axion ϕ_A couples to photons via the term in the action

$$\mathcal{S}_{A\gamma} = \int d^3x dt g_{A\gamma\gamma} \phi_A \mathbf{E} \cdot \mathbf{B} \quad (31)$$

where, \mathbf{E} is the electric field and \mathbf{B} is the magnetic field. We follow here the conventions of Ref. [25] in which the “free” terms in the axion action take the form

$$\mathcal{S}_A = \int d^3x dt \left[(1/2)(\partial_t \phi_A)^2 - (1/2)(\nabla \phi_A)^2 - (1/2)m_A^2 \phi_A^2 \right]. \quad (32)$$

- [32] J. Schwinger, “On Gauge Invariance and Vacuum Polarization,” *Phys. Rev.* **82**, 664 (1951). See Appendix B for the calculation of the spin precession frequency using the photon propagator $D_+(x, x')$ at leading order in quantum electrodynamics.
- [33] The photon propagator enters linearly in the quantum electrodynamic expression for the mass operator $M(x, x')$ of the muon interacting with its proper radiation field and the external magnetic field. The axion shift $\Delta D(x, x')$ of the photon propagator then carries over to a shift of the mass operator $\Delta M(x, x') = m_A^2 g_{A\gamma\gamma} \tilde{\phi}_A(q_A) M(x, x')$. In turn the spin precession frequency as well as the leading order quantum electrodynamic contribution to the rest-mass must shift in the same manner. They are simply the leading terms in the mass operator obtained by expanding $M(x, x')$ to leading order in the electromagnetic fine-structure constant $\alpha \approx 1/137$ [32].
- [34] Under C , PT and CPT , the shift Δa_μ , like the axion amplitude, does not change sign.
- [35] The consensus consists of the lattice quantum chromodynamic result $a_\mu^{\text{HLO}}(\text{QCD}) = (707.5 \pm 5.5) \times 10^{-10}$ [7] from the BMW collaboration, the dispersive result from the charged ρ^\pm vector meson resonance $a_\mu^{\text{HLO}}(\rho^\pm) = (703.0 \pm 4.4) \times 10^{-10}$ [9–11] from the BELLE and ALEPH collaborations, and the dispersive result from the neutral ρ^0 vector meson resonance $a_\mu^{\text{HLO}}(\rho^0) = ((379.5 \pm 3.0) + (322.5 \pm 2.9)) \times 10^{-10} = (702.0 \pm 5.9) \times 10^{-10}$ from the CMD-3 collaboration on resonance (first term) [8] and a recent compilation of off-resonant measurements (second term) [11]. These determinations are independent and mutually consistent. The weighted average gives the Standard Model value for the leading order hadronic contribution to muon spin precession $a_\mu^{\text{HLO}}(\text{SM}) = (704.1 \pm 3.0) \times 10^{-10}$.
- [36] The measurements from Runs 2 and 3 at Fermilab E989 [2] dominate the current world average for the muon spin precession frequency from experiment [2–4]

$$a_\mu(\text{Exp}) = (116\,592\,059 \pm 22) \times 10^{-11}. \quad (33)$$

The emerging consensus for the hadronic contribution $a_\mu^{\text{HLO}}(\text{SM}) = (7041 \pm 30) \times 10^{-11}$ [35] gives the best present estimate of the muon spin precession frequency within the Standard Model [6–11]

$$a_\mu(\text{SM}) = (116\,591\,919 \pm 35) \times 10^{-11}. \quad (34)$$

These estimates of the muon spin precession frequency create 3.4σ tension

$$\begin{aligned} a_\mu(\text{Exp}) - a_\mu(\text{SM}) &= (116\,592\,059 \pm 22) \times 10^{-11} \\ &- (116\,591\,919 \pm 35) \times 10^{-11} \\ &= (140 \pm 41) \times 10^{-11}. \end{aligned} \quad (35)$$

[37] For the muon beam at Fermilab E989 (FNAL) [2, 3], the volume is

$$V_\mu = 2\pi^2 R \sigma_x \sigma_y = 3.12 \times 10^4 \text{ cm}^3, \quad (36)$$

where, $R = 711$ cm is the radius of the central orbit of muons in the ring, $\sigma_x = 1.78$ cm is the radial width of the beam, and $\sigma_y = 1.25$ cm is the vertical width [3, 75, 76]. The average number of muons is

$$N_\mu = \frac{4}{9} N_0 e^{-t_{\text{fill}}/(\gamma\tau_\mu)} \approx \frac{4}{9} \times 4340 = 1930, \quad (37)$$

where, $N_0 \approx 6920$ is the number of muons in the ring at the start of the fill, and $t_{\text{fill}} \approx 30$ μsec is the time it takes to fill the ring [3, 75]. The muon life-time in the haloscope rest frame is $T_\mu = \gamma_\mu \tau_\mu = 64.4$ μsec , where, $\gamma_\mu \approx p_\mu/(m_\mu c) = 29.3$ is the muon time dilation factor, $p_\mu = 3.10$ GeV/c is the muon momentum, $m_\mu = 0.106$ GeV/c² is the muon rest mass, and $\tau_\mu = 2.20$ μsec is the muon life-time at rest [3]. For the measurements at Brookhaven E821 (BNL) [4], we estimate $N_\mu = 1290$, $\sigma_x = 2.10$ cm, $\sigma_y = 1.53$ cm (J. Mott, private communication). To find the shift of muon spin precession from halo axions, we first computed $|\Delta a_\mu(\text{FNAL})| = (165 \pm 10) \times 10^{-11}$ and $|\Delta a_\mu(\text{BNL})| = (161 \pm 10) \times 10^{-11}$ for each experiment using Eq. (3). Next we took the average of the two experiments to obtain Δa_μ , since the shifts essentially agree. The averages are weighted by the precision of the experiments: $\sigma_{a_\mu}(\text{BNL})/a_\mu = 540$ ppm [4] and $\sigma_{a_\mu}(\text{FNAL}) = 200$ ppm [2].

[38] Dispersive determinations of the hadronic leading order contribution based on the charged ρ^\pm vector meson resonance such as those by the BELLE [9] and ALEPH [10] detectors are not subject to the axion shift. The axion and the isoscalar ω vector meson are neutral. By charge conservation, only the neutral ρ^0 vector meson is effected by the axion shift.

[39] The axion coupling to the neutral ρ^0 and isoscalar ω vector mesons is analogous to the axion coupling to the electric \mathbf{E} and magnetic \mathbf{B} fields [31]. The coupling to the axion shifts the vector meson propagator $D_+^{\rho^\omega}(x, x')$ which enters the leading order hadronic contribution $a_\mu^{\pi\pi}$ in a manner analogous to the way the photon propagator $D_+(x, x')$ enters the leading order quantum electrodynamic contribution $a_\mu \approx \alpha/(2\pi)$ [32].

[40] The calculation of the hadronic leading order contribution a_μ^{HLO} from measurements of electrically neutral final state hadronic production is dominated by $a_\mu^{\pi\pi}$ the charged pion $\pi^+\pi^-$ production at the ρ^0 vector resonance [6]. However, off-resonant $\pi^+\pi^-$ production and hadronic production in other electrically neutral channels such as $\pi^+\pi^-\pi^0$ and $\pi^0\gamma$ must be included as well. A recent compilation of these other parts of the hadronic leading order contributions gives the result $a_\mu^{\text{HLO,other}} = (322.5 \pm 2.9) \times 10^{-10}$ [11].

[41] To get the coupling $g_{A\rho\omega}$ of the axion to the neutral ρ^0 and isoscalar ω vector mesons, we follow the analysis reviewed in Ref. [25] and set the ratio of axion couplings $g_{A\rho\omega}/g_{A\gamma\gamma} = g_{\pi\rho\omega}/g_{\pi\gamma\gamma}$ to match that of the neutral pion. Vector meson dominance [77] gives the pion ratio in terms of the ρ and ω vector meson partial widths Γ_ρ^{ee} and Γ_ω^{ee} for electron-positron pair production. The relevant meson parameters are as follows [12]:

$$m_\rho = 775 \text{ MeV},$$

$$\begin{aligned} m_\omega &= 783 \text{ MeV}, \\ \Gamma_\rho^{ee} &= \Gamma_\rho \times \text{B.R.}(\rho \rightarrow e^+e^-) \\ &= (147 \text{ MeV})(4.72 \times 10^{-5}) = 6.94 \text{ keV}, \\ \Gamma_\omega^{ee} &= \Gamma_\omega \times \text{B.R.}(\omega \rightarrow e^+e^-) \\ &= (8.68 \text{ MeV})(7.38 \times 10^{-5}) = 0.641 \text{ keV}. \end{aligned}$$

Using the meson parameters, we can find the vector meson coupling strengths [77]:

$$\begin{aligned} g_\rho^2/(4\pi) &= \alpha^2 m_\rho / (3\Gamma_\rho^{ee}) = 1.98, \\ g_\omega^2/(4\pi) &= \alpha^2 m_\omega / (3\Gamma_\omega^{ee}) = 21.7. \end{aligned}$$

These coupling strengths then give the ratio of the axion-meson coupling to the axion-photon coupling [25, 77]:

$$\frac{g_{A\rho\omega}}{g_{A\gamma\gamma}} = \frac{1}{\alpha} \sqrt{\frac{g_\rho^2}{4\pi} \frac{g_\omega^2}{4\pi}} = 8.98 \times 10^2. \quad (38)$$

[42] The vector meson propagator shift $\Delta D_+^{\rho^\omega}(x, x') = m_A E_\rho g_{A\rho\omega} \tilde{\phi}_A(q_a)$ follows by analogy to the shift of the photon propagator given in Eq. (4). The shift of the ρ^0 resonance part of the leading order hadronic contribution $\Delta a_\mu^{\pi\pi} = m_A E_\rho g_{A\rho\omega} \tilde{\phi}_A(q_a) a_\mu^{\pi\pi}$ has the same relative size as the shift of the vector meson propagator due to the linear dependence of $a_\mu^{\pi\pi}$ on $D_+^{\rho^\omega}(x, x')$ at leading order in the hadronic contribution. This linear dependence is analogous to that of a_μ on the photon propagator $D_+(x, x')$ [32].

[43] The luminous volume is $V_\rho = 8\pi\sigma_x\sigma_y\sigma_z$ and the crossing time is $T_\rho = 2\sigma_z/c$. The Standard Model value for the resonant part of the hadronic leading order contribution is roughly $a_\mu^{\pi\pi} \approx 380 \times 10^{-10}$ [6, 8]. The FNAL E989 axion shift of the muon spin precession frequency is $\Delta a_\mu(\text{FNAL}) = (165 \pm 10) \times 10^{-11}$ [37] and the muon beam parameters are $N_\mu = 1930$, $V_\mu = 3.12 \times 10^4$ cm³, and $T_\mu = 64.4$ μsec [37].

[44] F. Ambrosino *et al.* (KLOE Collaboration), Phys. Lett B **670**, 285 (2009).

[45] F. Ambrosino *et al.* (KLOE Collaboration), Phys. Lett B **700**, 102 (2011).

[46] F. Ambrosino *et al.* (KLOE Collaboration), Phys. Lett B **720**, 336 (2013).

[47] F. Ambrosino *et al.* (KLOE Collaboration), JHEP **03**, 173 (2018).

[48] To get the gap between CMD-3 and KLOE, we use the resonant $\pi^+\pi^-$ contribution $a_\mu^{\pi\pi}$ from electron-positron annihilation with center-of-mass energy $0.6 \text{ GeV} \leq \sqrt{s} \leq 0.88 \text{ GeV}$ in the window around the ρ^0 resonance given in Table 4 of Ref. [8]:

$$\begin{aligned} a_\mu^{\pi\pi}(\text{CMD3}) - a_\mu^{\pi\pi}(\text{KLOE}) &= ((3793 \pm 30) - (3606 \pm 21)) \times 10^{-11} \\ &= (188 \pm 37) \times 10^{-11}. \end{aligned} \quad (39)$$

[49] We assume $\Delta a_\mu^{\pi\pi}(\text{CMD3}) \approx 0$ that there is no significant axion shift of $a_\mu^{\pi\pi}(\text{CMD3})$ since it gives hadronic leading order contribution $a_\mu^{\text{HLO}}(\text{CMD3})$ that agrees with the emerging consensus [35] and the emerging consensus includes determinations that are not effected by the axion [38]. To get the axion shift of KLOE from the Standard Model, we evaluate the ρ energy $E_\rho = \sqrt{m_\rho^2 + p_\rho^2} = 805$ MeV in terms of its mass $m_\rho = 775$ MeV [41] and

momentum $p_p = (s - m_\rho^2)/(2\sqrt{s}) = 219$ MeV [78] where, $\sqrt{s} = m_\phi = 1020$ MeV [79] is the center-of-mass energy of the electrons and positrons at the DAΦNE collider. The beam parameters during the 2002 KLOE run at DAΦNE were as follows [78]: $\sigma_x(2002) = 2000 \mu\text{m}$, $\sigma_y(2002) = 20 \mu\text{m}$, and $\sigma_z(2002) = 3$ cm. For the 2006 run, we use the beam parameters reported by the KLOE collaboration to the Particle Data Group [79]: $\sigma_x(2006) = 260 \mu\text{m}$, $\sigma_y(2006) = 4.8 \mu\text{m}$, and $\sigma_z(2006) = 2$ cm. Using Eq. (10), we obtain the KLOE axion shifts $\Delta a_\mu^{\text{HLO}}(2002) = (299 \pm 18) \times 10^{-11}$ and $\Delta a_\mu^{\text{HLO}} = (35 \pm 2) \times 10^{-11}$. Taking the equal weight average gives the result $\Delta a_\mu^{\text{HLO}}(\text{KLOE}) = ((299 \pm 18) + (35 \pm 2))/2 \times 10^{-11} = (167 \pm 10) \times 10^{-11}$.

[50] Figure 1 shows the leading order quantum electrodynamic radiative correction to the electromagnetic vertex of the proton in water [80]:

$$\Delta g'_{p,\text{EM}} = \frac{\alpha}{\pi\epsilon} \approx \frac{1}{137 \times \pi \times 78.4} \approx 2.96 \times 10^{-5}. \quad (40)$$

This correction dominates the axion shift since the axion needs to couple to a virtual photon. By contrast, hadronic contributions dominate the full radiative correction to the electromagnetic vertex of the proton in liquid water [51]:

$$(g'_p - 2)/2 \approx 2.79 - 1 = 1.79. \quad (41)$$

Despite dominating the full electromagnetic vertex correction, these hadronic contributions do not contain the necessary virtual photon. Thus, they make a subdominant contribution to the axion shift of the proton spin precession frequency in water.

[51] W. D. Phillips, W. E. Cooke and D. Kleppner, Phys. Rev. Lett. **35**, 1619 (1975); *ibid.* **36**, 689 and 1473 (1976).

[52] The bulb of liquid water in Ref. [51] was a sphere of diameter 1.3 cm with volume

$$V_p = (4\pi/3)(1.3/2)^3 \text{ cm}^3 = 1.15 \text{ cm}^3. \quad (42)$$

The proton resonance line-width $\Delta\omega'_p = 2\pi \times 1.5$ Hz due to variation in the field strength over the sample volume gave effective spin coherence time

$$T_p \approx 1/\Delta\omega'_p = 0.11 \text{ sec}. \quad (43)$$

The temperature of the bulb $T = (34.7 \pm 0.1)^\circ\text{C} = 308$ K gave proton spin polarization

$$\begin{aligned} P_p &= \frac{\hbar\omega'_p}{kT} = \frac{4.14 \times 10^{-9} \text{ eV/MHz} \times 15 \text{ MHz}}{0.862 \times 10^{-4} \text{ eV/K} \times 308 \text{ K}} \\ &= 2.34 \times 10^{-6}, \end{aligned} \quad (44)$$

where, the precession frequency was $\omega'_p = 2\pi \times 42.8 \text{ MHz/T} \times 0.35 \text{ T} = 15 \text{ MHz}$ in magnetic field $B = 0.35 \text{ T}$ [51]. Using the proton volume V_p and proton polarization P_p , we find the effective proton number

$$\begin{aligned} N_p &= n_p V_p P_p \\ &= (6.69 \times 10^{22} \text{ cm}^{-3}) \times (1.15 \text{ cm}^3) \times (2.34 \times 10^{-6}) \\ &= 1.80 \times 10^{17}, \end{aligned} \quad (45)$$

where, we have used the proton number density in liquid water

$$\begin{aligned} n_p &= (1.00 \text{ g/cm}^3)(6.02 \times 10^{23} \text{ H}_2\text{O}/18.0 \text{ g})(2 p/\text{H}_2\text{O}) \\ &= 6.69 \times 10^{22} \text{ cm}^{-3}. \end{aligned} \quad (46)$$

Using Eq. (13), we find the shift of the proton spin precession frequency in water:

$$\begin{aligned} \Delta g'_p &= 2 \times \frac{(165 \pm 10) \times 10^{-11}}{78.4} \left(\frac{1.80 \times 10^{17}}{1.93 \times 10^3} \right)^{1/2} \\ &\times \left(\frac{1.15 \text{ cm}^3}{3.12 \times 10^4 \text{ cm}^3} \right)^{1/2} \left(\frac{0.11 \text{ sec}}{64.4 \times 10^{-6} \text{ sec}} \right)^{1/2} \\ &= (1.02 \pm 0.06) \times 10^{-4} \\ &\times \left(\frac{V_p}{1.15 \text{ cm}^3} \right) \left(\frac{T_p}{308 \text{ K}} \right)^{-1/2} \left(\frac{\Delta\omega'_p}{10^{-7} \omega'_p} \right)^{-1/2}, \end{aligned} \quad (47)$$

where, $\epsilon = 78.4$ [80] is the static dielectric constant in water and we have taken the muon beam parameters N_μ, V_μ, T_μ and the predicted shift Δa_μ from the Fermilab E989 muon spin precession measurement [37]. Taking the temperature derivative, we find the slope

$$\begin{aligned} \frac{1}{g'_p} \frac{dg'_p}{dT} &= -\frac{1}{2} \frac{\Delta g'_p}{g'_p T} = -(29.7 \pm 1.8) \frac{\text{ppb}}{\text{K}} \left(\frac{V}{1.15 \text{ cm}^3} \right) \\ &\times \left(\frac{T}{308 \text{ K}} \right)^{-3/2} \left(\frac{\Delta\omega'_p}{10^{-7} \omega'_p} \right)^{-1/2}, \end{aligned} \quad (48)$$

where, $g'_p \approx 5.58$ gives the slope in parts per billion (ppb) of g'_p [51].

[53] The internal magnetic field felt by valence electrons in their rest-frame is created within high atomic number atoms by the motion of the electrons at close to the speed of light through the static internal electric field created by the nucleus of the atom and screened by the core electrons.

[54] Atoms with mass m and temperature T moving in the optical lattice trap of radius r and height z trace out the volume

$$\begin{aligned} V_a &= \pi r^2 z \\ &= \sqrt{2}\pi^2 \left(\frac{w}{\lambda_L} \right)^2 \left(\frac{\lambda_L}{2\pi} \right)^3 \left(\frac{kT}{V_0} \right)^{3/2} \\ &= 5.5 \times 10^{-12} \text{ cm}^3 \left(\frac{T}{9 \mu\text{K}} \right)^{3/2} \left(\frac{V_0}{200 E_R} \right)^{-3/2} \\ &\times \left(\frac{E_R}{\hbar \times 2.0 \text{ kHz}} \right)^{-3} \left(\frac{m}{171 m_p} \right)^{-3/2} \left(\frac{w}{26.4 \lambda_L} \right)^2, \end{aligned} \quad (49)$$

where, the lattice photons have wavelength λ_L , the lattice laser has beam waist w , and the lattice has depth V_0 expressed in terms of the lattice recoil energy $E_R = \hbar^2/(2m\lambda_L^2)$. The thermal motion of the ultracold atoms in the trap has coherence time $T_a = \hbar/(kT)$ set by the temperature of the atoms.

[55] T. Kobayashi *et al.*, Phys. Rev. Lett. **129**, 241301 (2022). For the observations of the density shift of the optical lattice clock frequency with roughly the size predicted by Eq. (17), see Section 1.2 of the Supplementary Materials. The lattice photon wavelength $\lambda_L = 759$ nm gives recoil energy $E_R = \hbar \times 2.0$ kHz for ytterbium-171 atoms which have mass $m = 171 m_p$. The lattice had depth $V_0 = 200 E_R = 0.47 kT$ for atoms which typically had temperature $T = 9 \mu\text{K}$. The lattice laser beam had waist $w = 26.4 \lambda_L = 20 \mu\text{m}$ and there were typically $N_a = 100$ atoms in the trap (T. Kobayashi, private communication). In the main paper, the authors use $k_\alpha = -2.59$ for

the sensitivity to changes in the fine-structure constant for the line ratio $\nu_{\text{Yb}}/\nu_{\text{Cs}}$ of the ytterbium optical lattice clock frequency to the cesium-133 microwave clock frequency. However, the density shift due to modulating the ytterbium atom number occurs at fixed ν_{Cs} . In that case, the appropriate sensitivity $k_\alpha \approx 0.24$ is simply that of the ytterbium transition frequency [81].

- [56] In the presence of axions with amplitude $\tilde{\phi}_A(q_A)$, the equations of motion for the infrared magnetic field B_{IR} and the radio-frequency electric field E_{RF} have the following solution

$$E_{\text{RF}} = m_A^2 g_{A\gamma\gamma} \tilde{\phi}_A(q_A) B_{\text{IR}}, \quad (50)$$

where, the mass of the axion $m_A c^2/\hbar = \omega_A = \omega_{\text{IR}} + \omega_{\text{RF}}$ relates the frequency ω_{IR} of the infrared light and the frequency ω_{RF} of the radio waves. The radio-frequency power $P_{\text{RF}} = (1/2) \times E_{\text{RF}}^2/(2Z_0)$ with the polarization that excites the resonance is half of the total amount created by the unpolarized infrared power $P_{\text{IR}} = (B_{\text{IR}}c)^2/(2Z_0)$, where, $Z_0 = \sqrt{\mu_0/\epsilon_0} \approx 377 \Omega$ is the impedance of the vacuum.

- [57] The tunable continuous-wave external cavity diode laser (Sacher Lasertechnik TEC-500-2400-003-M) has infrared wavelength range 2300 nm – 2500 nm that includes the predicted Compton wavelength of dark matter $\lambda_A = 2440 \pm 19$ nm and it has line-width $\Delta\nu_{\text{IR}} = 1$ MHz. For a recent demonstration of phase coherence with infrared laser beams enlarged to a radius ≈ 5 mm comparable to the beam waist $c/\omega_c = 5.3$ mm $(B/0.32 \text{ T})^{-1}$ needed to see dark matter with plasma haloscopy [59] and the beam diameter $D = 1$ cm needed for microwave [60] and bend magnet haloscopy [63], see Ref. [82], Supplementary Materials, pg. 2.
- [58] K. Hoshino, J. Nucl. Sci. and Tech. **27**, 391 (1990) describes electron cyclotron heating in magnetically confined laboratory plasma with $\beta = 0.8$, $L = 100$ cm, $T = 12,000$ K, and $B = 0.32$ T.
- [59] For light and electrons propagating along the magnetic field, only right-handed circularly polarized light is absorbed by the electron cyclotron motion. Left-handed light passes through without being absorbed. For an unpolarized incoming beam, the out-going beam has circular polarization $(P_L - P_R)/(P_L + P_R) = \Delta P_{\text{IR}}/P_{\text{IR}}$ given by Eq. 19, where, P_L is the left-handed and P_R is the right-handed transmitted infrared power. Electrons in a warm, magnetically confined plasma at temperature T and magnetic field strength B have density

$$\begin{aligned} n_e &= \beta \frac{B^2}{2\mu_0 kT} \\ &= 2.0 \times 10^{17} \text{ cm}^3 \left(\frac{\beta}{0.8}\right) \left(\frac{T}{12,000 \text{ K}}\right)^{-1} \left(\frac{B}{0.32 \text{ T}}\right)^2, \end{aligned} \quad (51)$$

where, $\mu_0 = 4\pi \times 10^{-7} \text{ T}^2 \text{ m}^3 \text{ J}^{-1}$ is the magnetic permeability of the vacuum [72], $k = 1.38 \times 10^{-23} \text{ J/K}$ [72] is the Boltzmann constant, and β is the ratio of the electron pressure to the magnetic energy density. Passing the plasma through the bore of a solenoid magnet gives the coherent volume

$$V_e = \pi(c/\omega_c)^2 L = 89 \text{ cm}^3 \left(\frac{B}{0.32 \text{ T}}\right)^{-2} \left(\frac{L}{100 \text{ cm}}\right), \quad (52)$$

where, ω_c is the cyclotron frequency, L is the length of the bore, and the laser beam waist is set by the reduced

wavelength $c/\omega_c = 5.3$ mm $(B/0.32 \text{ T})^{-1}$ of the radio-frequency electromagnetic waves at electron cyclotron resonance. The coherent line-width $\Delta\nu_{\text{IR}}$ of the infrared laser sets the coherence time

$$T_e = \frac{1}{2\pi\Delta\nu_{\text{IR}}} = 0.16 \mu\text{sec} \left(\frac{\Delta\nu_{\text{IR}}}{1 \text{ MHz}}\right)^{-1}. \quad (53)$$

- [60] The volume of the infrared beam $V_{\text{IR}} = (\pi/4)D^2L$ is fixed by the beam diameter D and the cavity length L . The coherence time $T_{\text{IR}} = 1/(2\pi\Delta\nu_{\text{IR}})$ comes from the infrared laser line-width $\Delta\nu_{\text{IR}}$. The radio-frequency power P_{IR} combines with the receiver noise temperature T_S and the integration time T_{int} to give the signal-to-noise ratio [83]

$$\text{SNR} = \frac{P_{\text{RF}}}{kT_S} \sqrt{\frac{T_{\text{int}}}{\Delta\nu_{\text{IR}}}}. \quad (54)$$

The total search time $T_A = T_{\text{int}}\Delta m_A c^2/(h\Delta\nu_{\text{IR}})$ is set by the width of the window $\Delta m_A c^2 = 4 \times 10^{-3} \text{ eV} = h \times 1.0 \text{ THz}$ for the axion mass given in Eq. 2.

- [61] The typical microwave cavity has length $L = 112$ cm and is read out by a receiver with noise temperature $T_S = 77$ K set by the boiling point of liquid nitrogen. See for example the cavity and receiver described in Ref. [84].
- [62] In the presence of axions with amplitude $\tilde{\phi}_A(q_A)$, the equations of motion for the infrared electric field E_{IR} and the static magnetic field B_{DC} have the following solution

$$E_{\text{IR}} = m_A^2 g_{A\gamma\gamma} \tilde{\phi}_A(q_A) B_{\text{DC}}, \quad (55)$$

where, the mass of the axion $m_A c^2/\hbar = \omega_A = \omega_{\text{IR}}$ gives the frequency of the infrared light and the impedance $Z_0 = \sqrt{\mu_0/\epsilon_0} \approx 377 \Omega$ [72] of the vacuum gives the infrared power $P_{\text{IR}} = E_{\text{IR}}^2/(2Z_0)$. The infrared electric field E_{IR} is polarized along the static magnetic field B_{DC} .

- [63] The infrared cavity fills the volume $V_B = (\pi/4)D^2L$ within the bend magnet of length L defined by the beam diameter D of the infrared laser used to tune the cavity. The tune laser is polarized with its electric field perpendicular to the static magnetic field B_{DC} and a crossed linear polarizer oriented parallel to B_{DC} at the cavity exit transmits to the photodiode reading out the infrared power P_{IR} only the infrared photons created within the cavity by dark matter. The infrared cavity has coherence time $T_{\text{IR}} = 1/(2\pi\Delta\nu_{\text{IR}})$ when it is tuned to a laser with line-width $\Delta\nu_{\text{IR}}$. For each frequency in the window $\Delta\omega_A = 2\pi \times 1.0 \text{ THz}$ around the dark matter resonance $\omega_A = 2\pi \times (122.7 \pm 1.0) \text{ THz}$, we have integration time $T_{\text{int}} = T_A \times \Delta\omega_A/(2\pi\Delta\nu_{\text{IR}})$, where T_A is the total time taken to scan the window assuming T_{int} is much longer than the time it takes to lock the cavity to the laser at a given wavelength.

- [64] The two-stage thermoelectrically cooled indium gallium arsenide photodiode (Hamamatsu G12183-230K) with photosensitive area $S_{\text{IR}} = \pi \times (3 \text{ mm})^2 = 2.83 \times 10^{-5} \text{ m}^2$ has typical noise equivalent power $\text{NEP}_A = (1.15/1.3) \times \text{NEP}_{\text{peak}} = 5.3 \times 10^{-13} \text{ W/Hz}^{1/2}$ at the Compton wavelength of dark matter $\lambda_A = (2.44 \pm 0.02) \mu\text{m}$, where NEP_{peak} is the typical value for the most photosensitive wavelength $\lambda_{\text{peak}} \approx 2.3 \mu\text{m}$ in the photodiode's spectral response range from $0.9 \mu\text{m}$ to $2.55 \mu\text{m}$. For integration time T_{int} , we get the signal-to-noise ratio $\text{SNR} = P_{\text{IR}} T_{\text{int}}^{1/2}/\text{NEP}_A$.

- [65] Typical magnetic dipole bend magnets have magnetic field strength $B_{DC} = 1$ T and length $L = 100$ cm. See for example Ref. [85] in which an infrared optical cavity was created within a bend magnet from the proton storage ring of the former HERA electron-proton collider at DESY in Hamburg.
- [66] R. de Sousa and J. E. Moore, Phys. Rev. B **77**, 012406 (2008).
- [67] D. Talbayev, S. A. Trugman, Seongsu Lee, Hee Taek Yi, S.-W. Cheong, and A. J. Taylor, Phys. Rev. B **83**, 094403 (2011).
- [68] The electromagnon θ resonates when the terahertz electric field E_{THz} is perpendicular to the spin cycloid plane in BiFeO₃. This plane is defined by the spontaneous polarization P_{DC} and the cycloid wavevector: See Eq. (10), Fig. 2, and accompanying discussion on pg. 3 of Ref. [66]. The axion converts the magnetic field B_{IR} in the incident infrared light into a parallel terahertz frequency electric field E_{THz} . The infrared light gets absorbed when E_{THz} resonates with the electromagnon θ . This happens when B_{IR} is perpendicular to the spin cycloid plane.
- [69] The absorption coefficient $\alpha(\omega)$ for electromagnetic waves of frequency ω gives the attenuation rate for the decrease of the transmitted light intensity $I(z) = I_0 \exp(-\alpha(\omega)z)$ as a function of the thickness z of the sample for incident light with intensity I_0 . See M. Dressel and G. Gruner, *Electrodynamics of Solids*, Cambridge University Press, Cambridge, UK (2002), pg. 26. Similarly, the refractive index $n(\omega)$ gives the wavevector $k(\omega) = n(\omega)\omega/c$ for electromagnetic waves of frequency ω , where, c is the vacuum speed of light. See *ibid.*, pg. 24.
- [70] The typical room-temperature electromagnon absorption coefficient is $\alpha(\omega_\theta) = 10^7 \text{ cm}^{-1}$ while the index of refraction is $n(\omega_{A\theta}) = 10$ [67]. The electrons that participate in the electromagnon in BiFeO₃ have density

$$n_\theta = \frac{\rho N_A}{\mu} = \frac{(8.22 \text{ g/cm}^3)(6.02 \times 10^{23})}{313} = 1.58 \times 10^{22} \text{ cm}^{-3}, \quad (56)$$

where, ρ is the mass density of BiFeO₃, N_A is the Avogadro number [72], and μ is the molar mass of BiFeO₃. The typical electromagnon line-width $\Delta\nu_\theta \approx 5.3$ GHz [67] at room temperature sets the coherent life-time

$$T_\theta = \frac{1}{2\pi\Delta\nu_\theta} = 30 \text{ ps} \left(\frac{\Delta\nu_\theta}{5.3 \text{ GHz}} \right)^{-1}. \quad (57)$$

The diameter $d = 0.3$ cm of a ferroelectric domain within a single crystal sample sets the spot size for the light shining through the sample of thickness $t = 0.1$ cm to

give the coherent volume

$$V_e = \frac{1}{4}\pi d^2 t = 7.1 \times 10^{-3} \text{ cm}^3 \left(\frac{d}{0.3 \text{ cm}} \right)^2 \left(\frac{t}{0.1 \text{ cm}} \right). \quad (58)$$

- [71] M. E. Peskin and D. V. Schroeder, *An Introduction to Quantum Field Theory*, Perseus, Cambridge, MA (1995).
- [72] D. B. Newell *et al.* (CODATA), Metrologia **55**, L13 (2018).
- [73] A. Ceccucci, Z. Ligeti, and Y. Sakai, *12. CKM Quark-Mixing Matrix*, pg. 262 in Ref. [12].
- [74] Z. Fodor, C. Hoelbig, S. Krieg *et al.*, Phys. Rev. Lett. **117**, 082001 (2016).
- [75] T. Albahri *et al.* (Muon $g-2$ Collaboration), Phys. Rev. Accel. Beams **24**, 044002 (2021).
- [76] T. Albahri *et al.* (Muon $g-2$ Collaboration), Phys. Rev. D **103**, 072002 (2021).
- [77] R. P. Feynman, *Photon-Hadron Interactions*, Addison-Wesley, Redwood City, CA (1972), pgs. 82–85 introduce the vector meson coupling strengths

$$g_V = \alpha \sqrt{4\pi m_V / (3\Gamma_V^{ee})} \quad (59)$$

for $V = \rho, \omega$ and pgs. 96–97 express the pion amplitude ratio $g_{\pi\rho\omega}/g_{\pi\gamma\gamma} = g_\rho g_\omega / (4\pi e^2)$ in terms of these couplings and the electric charge e . Note that $e^2 = \alpha \approx 1/137$ in Feynman's conventions.

- [78] F. Ambrosino *et al.* (KLOE Collaboration), Eur. Phys. J. C **47**, 589 (2006).
- [79] V. Shiltsev and F. Zimmerman, 32. High Energy Collider Parameters in Ref. [12]
- [80] D. P. Fernandez, Y. Mulev, A. R. Goodwin and J. M. H. Levelt Sengers, J. Phys. Chem. Ref. Data **24**, 33 (1995). Table 2 gives the static dielectric constant $\epsilon = 78.43 \pm 0.10$ for liquid water at room temperature $T = 298.14$ K and atmospheric pressure $P_a = 10^5$ Pa by averaging over published measurements of the dielectric response at frequencies ranging from 100 Hz to 40 GHz. The quoted uncertainty is the population standard deviation of these measurements about their average value.
- [81] V. V. Flambaum, D. B. Leinweber, A. W. Thomas, and R. D. Young, Phys. Rev. D **69**, 115006 (2004). Section III gives $\Delta\nu_{Cs}/\nu_{Cs} = 2.83 \Delta\alpha/\alpha$ for the sensitivity of the cesium-133 microwave clock frequency to the electromagnetic fine-structure constant. Combining with the sensitivity $k_\alpha = -2.59$ of the line ratio ν_{Yb}/ν_{Cs} [55], we obtain the ytterbium-171 optical lattice clock sensitivity $\Delta\nu_{Yb}/\nu_{Yb} = (2.83 - 2.59) \Delta\alpha/\alpha = 0.24 \Delta\alpha/\alpha$.
- [82] R. Cardman and G. Raithel, Phys. Rev. Lett. **131**, 023201 (2023).
- [83] R. H. Dicke, Rev. Sci. Instrum. **17**, 268 (1946).
- [84] C. Bartram *et al.* (ADMX Collaboration), Phys. Rev. Lett. **127**, 261803 (2021).
- [85] K. Ehret *et al.* (ALPS Collaboration), Nucl. Instrum. Meth. A **612**, 83 (2009).